
Microhardness and Indentation Fracture of Potassium Dihydrogen Phosphate (KDP)

Introduction

Potassium dihydrogen phosphate (KDP) is an important electro-optic tetragonal crystal. For example, it is used as a photonic material in the third-harmonic generation (THG) to reduce light wavelength from 1.054 μm to 351 nm. Microindentation has been used to measure the Vickers and Knoop hardness of KDP and the resulting cracking on (100) and (001) faces. Hardness anisotropy on the (001) face, or among the (100) and (001) faces, was found to be small (about 20%). An indentation size effect for both Vickers and Knoop hardness for indenting loads in the range of 25 to 200 g was observed. The large-load Vickers hardness was estimated as 1.4 ± 0.1 GPa. Anisotropy in the crack sizes on (100) and (001) faces was also observed. Cracks were longer on (100) faces, scaling like $c \sim P^{2/3}$; cracks on (001) faces were shorter, scaling like $c \sim P^{1/2}$. Assuming elastic and plastic isotropy, crack sizes were analyzed and fracture toughness K_c was extracted. An approximate model for analyzing crack-load microindentation data in tetragonal crystals is presented in this article. The model uses the minimum elastic modulus of the material. The effect of the isotropy assumption on the extracted fracture toughness is estimated at about 33%, with a 23% contribution from elastic anisotropy and 10% from the slip system plastic anisotropy. Strain-rate effects are identified as important aspects of KDP deformation, especially in laser damage applications.

One of the limiting factors in the use of KDP in THG is its susceptibility to laser damage, a process that couples light absorption with thermal and mechanical effects. (For a summary of the electro-optical properties, see Milek and Neuberger.¹)

KDP crystals are water soluble and brittle. Above its ferroelectric Curie temperature (123 K) the crystal structure of KDP is tetragonal, lacking a center of inversion. KDP is optically uniaxial with the optic axis along the tetragonal z axis or [001] direction. At room temperature the lattice constants are $a = 0.7453$ nm and $c = 0.6975$ nm, as cited in Ref. 1. The natural habit of crystals grown from solution is a tetragonal prism combined with a tetragonal bipyramid. The prism faces are (100) and (010) planes. The prism axis is [001].

KDP is relatively soft and brittle as compared to other optical materials, including glasses. In this article microhardness and indentation cracking fracture measurements of KDP indented on crystal planes (100) and (001) are summarized.

Kishan Rao and Sirdeshmukh² measured the Vickers microhardness of KDP at loads of 50 and 100 g, reporting a value of $H_v = 1.43$ GPa for indentation normal to {100} planes (what they called “ a -direction”) and 1.29 GPa for indentation normal to {001} planes (“ c -direction”). Their error was reported as $\pm 4\%$. Anbukumar *et al.*³ also measured the Vickers hardness of {100} planes of KDP. They reported hardness in the range of 1.77 to 1.57 GPa for loads in the range of 5 to 50 g and an indentation size effect (ISE) where the hardness decreased with increased load.

Shaskol'skaya *et al.*⁴ and Guin *et al.*⁵ reported measurements of both hardness and cracking in the Vickers measurements of KDP and $\text{KD}_{2x}\text{H}_{2-2x}\text{PO}_4$ (deuterated KDP, with $x = 0$ to 0.95). They used loads of 50 to 200 g and reported a hardness reduction from 1.44 GPa to 1.22 GPa as the extent of deuteration x increased from 0 to 0.95. Shaskol'skaya *et al.*⁴ also measured the length of cracks (tip-to-tip distance $2c$) due to Vickers indents. They observed that $(2c)/D$ varied from 3.87 to 3.61 as x increased from 0 to 0.95. They also reported a value of 51 MPa for the microstrength $P/(2c)^2$ of both KDP and 95% deuterated KDP.

Guin *et al.*⁵ reported measurements similar to those of Shaskol'skaya.⁴ They also identified two types of slip systems in KDP: the first system consisted of slip planes (110), (101), (112) and (123) with a common Burgers vector $\langle 111 \rangle / 2$; the second slip system was identified as (010)[100].

More recently, Marion⁶ has reported measured values of fracture toughness in KDP crystals. Marion apparently used the direct crack method described by Anstis *et al.*,⁷ although the measured data were not described. Marion⁶ reported fracture toughness K_c of $0.2 \text{ MPa}\cdot\text{m}^{1/2}$, as well as $0.09 \text{ MPa}\cdot\text{m}^{1/2}$ along the weakest direction (longest crack). No crystallo-

graphic orientation of the indented faces was reported, however, nor was the applicable elastic constant (modulus) given.

Given the importance of KDP in third-harmonic generation for 351-nm-wavelength laser systems, a systematic study of indentation hardness (Vickers and Knoop) and microindentation cracking in KDP is described below.

Measurements

Vickers indentation was used to measure the indentation size effect on H_V and also to extract the fracture toughness from the measured dependence of crack size on indenting load. Vickers hardness on (100), (010), and (001) planes of single-crystal KDP was measured at room temperature with a Tukon Microhardness Tester equipped with a video image-capture camera. Typical descent rate of the indenter is about 1 mm/min.

The KDP crystal was provided by a commercial vendor and had been grown from the solution. The crystal surfaces were polished by conventional means with nonaqueous slurries to optical standards. Although surface roughness was not directly measured, it was estimated to be approximately 3 to 5 nm (rms).

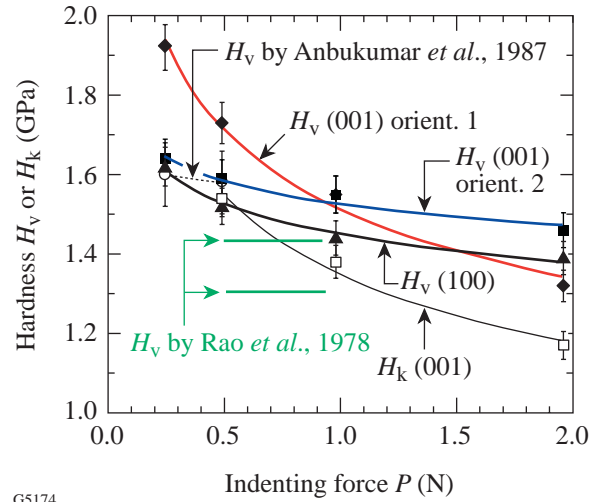
The indentation load was in the range of 2 to 200 g, and each load was applied for 15 s. Five indentations were performed at each load. The indentation diagonal D and crack size $2c$ (tip-to-tip distance) were measured with an optical microscope with a 50 \times objective lens. For the Vickers indentation of (100) and (010) planes, the indenter diagonals were along the principal directions of the type $\langle 100 \rangle$. No differences were observed in the indentation diagonal or crack size of (100) and (010) faces.

For the indentation of (001) planes, we selected two indenter orientations: in orientation (1), the indenter diagonals were parallel to [100] and [010]; in orientation (2), the indenter sides were along [100] and [010].

Figure 86.63 shows the measured hardness over the range of indenting loads used. Figure 86.64 shows the measured crack size for Vickers indentation of (100) and (001) faces. The crack-to-indent ratio $c/(D/2)$ varied from 2 to 4.5, depending on load and orientation.

Knoop indentation was used to measure the indentation size effect on Knoop hardness and also the hardness anisotropy of the (001) faces. For the indentation size effect (loads of 50 to

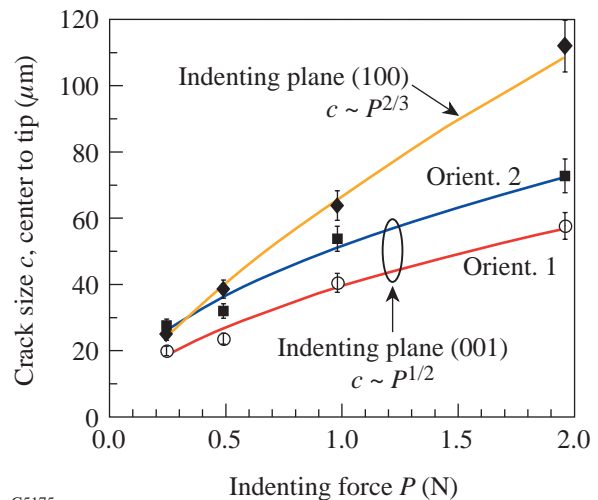
200 g), the indenter's long diagonal was along [010]. These results are included in Fig. 86.63.



G5174

Figure 86.63

Variation of measured hardness (Vickers and Knoop) with load for KDP at room temperature. Vickers indentation was done on faces (100) and on indenter orientations (1) and (2) on the (001) faces. Orientation (1) had the indent diagonals parallel to (100) and (010). Orientation (2) had the indent edges parallel to (100) and (010). Also shown are Vickers measurements by Anbukumar *et al.*³ and Rao *et al.*² Guin *et al.*⁵ reported Vickers hardness 1.45 GPa at 200 g.



G5175

Figure 86.64

Variation of indentation crack size c with indenting load. The tip-to-tip surface crack length is $2c$.

For the hardness anisotropy, we used a load of 50 g and measured the variation of H_k with orientation θ of the Knoop indenter with respect to the indented surface. Angle $\theta = 0^\circ$ corresponds to the indenter long diagonal along the [010] direction. The angle θ was changed in increments of 10° from $\theta = 0^\circ$ to 90° . The hardness anisotropy is shown in Fig. 86.65.

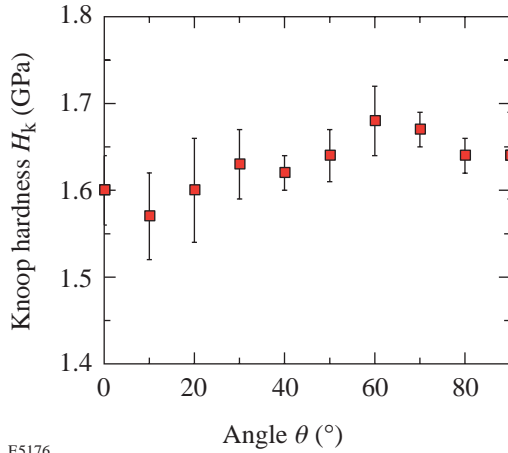


Figure 86.65
Dependence of Knoop hardness on angle θ of indent on the (001) plane. $\theta = 0$ corresponds to the Knoop diagonals being along (100) and (010).

Results

The measured Vickers hardness is seen to vary between 1.7 and 1.4 GPa over the indenting load range of 50 to 100 g. This hardness range is consistent with the measurements of Rao *et al.*² over the same load range. Our measurements are also consistent with those of Anbukumar *et al.*³ over the load range of 25 to 50 g, and with Guin *et al.*⁵ and Shaskol'skaya *et al.*⁴ who reported a hardness of 1.45 GPa at a load of 200 g.

The measured Vickers hardness brings up two questions: What is the relative hardness of (100) and (001) faces? What is the relative hardness of orientations (1) and (2) of the indenter on face (001)?

Our results show that for loads less than 150 g, (001) faces are harder than (100) faces by as much as 14% at lower loads. On (001) faces, orientation (1) is harder than orientation (2), by as much as 10%. At loads of about 200 g, however, both faces and both orientations have hardness in the range 1.4 ± 0.1 GPa; therefore, this value may be used as the load-independent, orientation-insensitive Vickers hardness of KDP.

Our results also show that the Knoop hardness on the (001) face is not strongly anisotropic. The variation of hardness with direction is seen to be less than 10%.

No analysis is available to convert measured micro-indentation crack sizes to fracture toughness in tetragonal crystals. The only available analysis is for isotropic materials, such as glasses or polycrystalline ceramics (see Ref. 8). Therefore, to convert our direct measurements of indentation crack size to a fracture toughness, we shall assume that KDP can be described by an equivalent isotropic Young's modulus $E = 38.7$ GPa. This value is the mean of the Reuss and Voigt averages for the Young's modulus, with the derivation presented in the Appendix. We have analyzed the microindentation crack measurements (indentation diagonal D , tip-to-tip crack size $2c$) using the model of Evans⁹ and Anstis *et al.*⁷ The comparative merits and applicability of various models to extract the fracture toughness by microindentation cracking in optical glasses and brittle ceramics have been discussed by Ponton and Rawlings^{10,11} and Lambropoulos *et al.*¹²

Evans⁹ used dimensional analysis and curve fitting over a range of $c/(D/2)$ from 1.5 to 7 and for many polycrystalline ceramic materials; thus, this model should be applicable to both short and long indentation cracks. According to the Evans model,⁹

$$K_c = H\sqrt{D/2} \left(\frac{E}{H}\right)^{0.4} 10^{f(x)}, \quad x = \log_{10}\left(\frac{c}{D/2}\right), \tag{1}$$

$$f(x) = -1.59 - 0.34x - 2.02x^2 + 11.23x^3 - 24.97x^4 + 16.23x^5,$$

where K_c is the fracture toughness, H is the hardness, D is the indentation diagonal, E is the Young's modulus, and c is the half-crack size. Lankford¹³ included Al_2O_3 , soda-lime silicate glass, and NaCl to the materials analyzed by Evans.⁹

Anstis *et al.*⁷ examined various glasses (glass-ceramic, soda-lime, aluminosilicate, lead alkali), polycrystal Al_2O_3 and sapphire, Si_3N_4 , SiC, Ca-PSZ ZrO_2 , Si, and SiC/Co and concluded that

$$K_c = (0.016 \pm 0.002) \left(\frac{E}{H}\right)^{1/2} \frac{P}{c^{3/2}}. \tag{2}$$

The Anstis model is based on the assumption that the observed surface cracks are surface traces of sufficiently large radial cracks, so that $c \sim P^{3/2}$. On the other hand, the Evans model is applicable for both shorter near-surface cracks, where $c \sim P$, and deeper radial cracks.

As an example of this approach, when the data by Shaskol'skaya *et al.*⁴ or Guin *et al.*⁵ are analyzed via the Evans model and with $E = 38.7$ GPa, they yield $K_c = 0.24 \pm 0.04$ MPa.m^{1/2} at the indentation load of 200 g. The Anstis model leads to $K_c = 0.17 \pm 0.03$ MPa.m^{1/2} over the same increase of indentation load. The Anstis model predictions are in agreement with the reported values of 0.09 to 0.20 MPa.m^{1/2} by Marion.⁶ Note, however, that the work of neither Shaskol'skaya *et al.*⁴ nor Guin *et al.*⁵ describes the orientation of the indented planes or the orientation of the indenter with respect to the indented plane.

The results of our data analysis using the Evans model are shown in Fig. 86.66, where we have used $E = 38.7$ GPa. We observe that the crack-to-indent aspect ratio $2c/D$ is in the range of 2 to 4.5, therefore within the range of applicability of the Evans model. It is seen that the computed fracture toughness K_c of indenting the (001) planes is higher than that when indenting the (100) planes. It is also observed that smaller crack sizes apparently produce higher fracture toughness. For $2c/D$ values of 3 or higher, however, it is seen that the fracture toughness becomes independent of the geometry of the indent producing the cracks. For completeness, Fig. 86.66 shows the (average) \pm (one standard deviation) of the computed fracture toughness for each of the two orientations (1) and (2) on faces (001), as well as that for face (100). The standard deviation was computed from the fracture toughness variation over all the indenting loads used. The results for the two orientations of face (001) overlap, while exceeding that for (100).

The comparisons of the models by Evans⁹ and Anstis *et al.*⁷ are shown in Fig. 86.67. Both results are based on using Young's modulus $E = 38.7$ GPa. We observe that the Evans model predicts fracture toughness that is a factor of 1.2 to 1.45 higher than the predictions of the Anstis model; however, both models give the same qualitative ranking of the data.

Discussion

The analysis above rests on two important assumptions. The first assumption is that the anisotropic KDP crystals can be analyzed for fracture toughness using an equivalent isotropic Young's modulus.

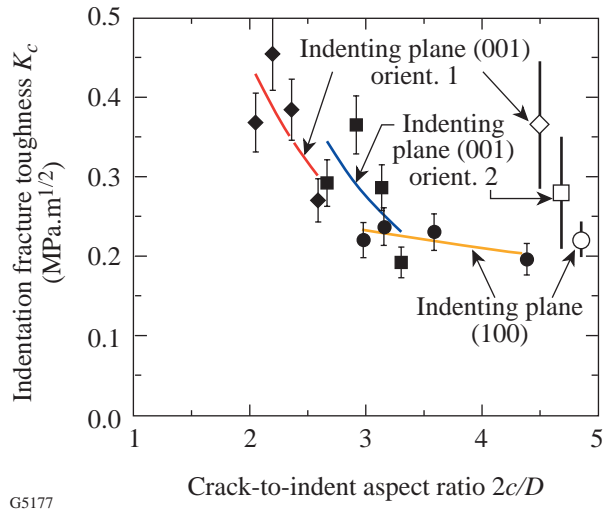


Figure 86.66 Dependence of fracture toughness computed via the Evans model⁹ on the crack-to-indent aspect ratio $2c/D$, using the average Young's modulus $E = 38.7$ GPa. Error bars on the data points reflect measurement uncertainty at each crack size. The thick vertical bars on the right show the (average) \pm (one standard deviation) for each indent orientation. The standard deviations shown on these bars reflect the variation of the fracture toughness over the whole range of indenting loads. To convert these values of fracture toughness to those with the minimum Young's modulus of $E = 20.4$ GPa, multiply these values by 0.774.

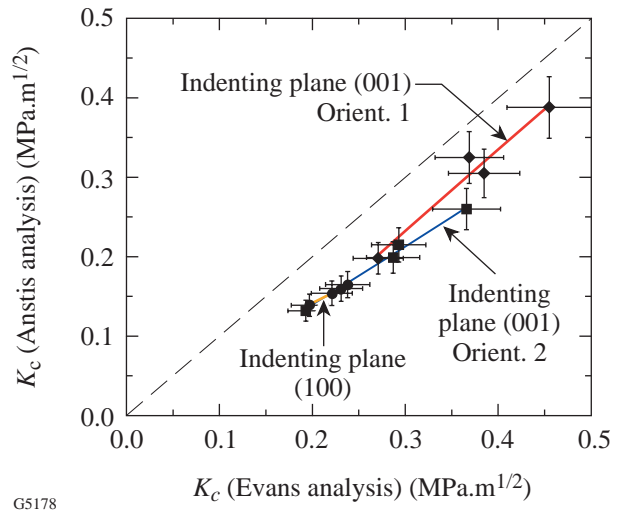


Figure 86.67 Comparison of prediction of fracture toughness by the Evans model⁹ and the Anstis *et al.*⁷ Results are for $E = 38.7$ GPa. The dashed straight line is a line of slope 1.

To estimate the effect of such an assumption, for example, on the predictions by the Evans model, we observe that that model uses the term $(E/H)^{0.4}$. As the unconstrained Young's modulus E varies from 20.4 to 65 GPa, we conclude that the minimum fracture toughness corresponds to the lowest Young's modulus of 20.4 GPa. This, in turn, leads to a change in K_c by $(20.4/38.7)^{0.4} = 0.774$. Therefore, the effect of elastic anisotropy is estimated to be about 23% on the computed fracture toughness. These results are summarized in Table 86.V. In our data, we give the uncertainty over all the indenting loads used. It is seen that the Anstis *et al.* model,⁷ when used in conjunction with the minimum Young's modulus of 20.4 GPa, yields fracture toughness in the range of 0.09 ± 0.02 to 0.22 ± 0.06 MPa.m^{1/2}, in agreement with the values 0.09 to 0.2 MPa.m^{1/2} cited by Marion.⁶

The other important assumption is that the material can be described as an elastic-plastic solid. With a melting point of $T_m = 525.6$ K, the room temperature at which the tests were conducted represents a homologous temperature of $293/525.6 = 0.57$. At such a relatively high temperature, and under the action of the high compressive stresses due to indentation, it is expected that KDP may deform by a variety of mechanisms, including dislocation glide on crystallographic slip systems, or power-law creep by dislocation climb/glide. At temperatures of about 110°C, KDP is known to exhibit macroscopic plasticity in a uniaxial compression.⁵ The room-temperature compressive yield stress does show anisotropy, being 140 MPa for compression along [100], 100 MPa along [110], and 130 MPa for compression along [001]. At 110°C, these values are

reduced by a factor of about 10;⁵ therefore, anisotropy under uniaxial conditions is about 20% of the uniaxial compressive yield stress. The anisotropic variation of Knoop hardness that we have measured on the (001) faces was seen to be within 10% of the average value. Likewise, the largest observed difference in Vickers hardness of (100) and (001) faces was no more than about 10%. Therefore, a total variation of 20% in hardness due to crystallographic anisotropy is expected, consistent with the anisotropy of the uniaxial compressive yield stress. On the other hand, as Eqs. (3) and (4) show, a 20% variation in hardness is expected to lead to a variation in the computed fracture toughness of about 10%.

Thus, the estimates of the effects of the Young's modulus anisotropy and hardness anisotropy, when combined, lead to a difference of about 33% in the fracture toughness as computed by an isotropic elastic-plastic model such as by Evans⁹ or Anstis *et al.*⁷

On the other hand, at a homologous temperature of 0.57 with respect to the melting point, power-law creep is a time-dependent process. Now, the strain rate depends on stress via a power law of exponent in the range of 3 to 8. In our experiments we have imposed a fixed strain rate, as determined by applying the indentation load for 15 s on the KDP faces. In typical laser-damage applications, the laser pulse duration over which damage accumulates is of the order of 10 ns, implying, therefore, that the applicable strain rates are much higher than those in indentation.

Table 86.V: Calculated fracture toughness K_c (Mpa.m^{1/2}) for KDP.

Indents on	Using average $E = 38.7$ GPa		Using minimum $E = 20.4$ GPa	
	Evans model ⁹	Anstis <i>et al.</i> model ⁷	Evans model ⁹	Anstis <i>et al.</i> model ⁷
(100) plane	0.22 ± 0.02	0.13 ± 0.03	0.17 ± 0.02	0.09 ± 0.02
(001) plane, indent orientation (1)	0.37 ± 0.08	0.30 ± 0.08	0.29 ± 0.06	0.22 ± 0.06
(001) plane, indent orientation (2)	0.28 ± 0.07	0.19 ± 0.06	0.22 ± 0.05	0.14 ± 0.04
Shaskol'skaya <i>et al.</i> ⁴	0.24 ± 0.04	0.17 ± 0.03	0.19 ± 0.03	0.12 ± 0.03
As cited in Marion ⁶	0.09–0.20 Using direct crack method of Anstis <i>et al.</i> ⁷ but with no information on E value used.			

Given the lack of data describing the dependence on stress and temperature of the deformation mechanisms of KDP, the strain-rate effects are more difficult to estimate. The development of deformation mechanism maps for KDP is thus an area identified for future research.

ACKNOWLEDGMENT

We wish to thank Prof. Stephen D. Jacobs and Mr. Douglas Smith, both of the Laboratory for Laser Energetics at the University of Rochester, for many discussions and suggestions and sample preparation.

Appendix A: Elastic Anisotropy of KDP

The elastic behavior of the single-crystal KDP is characterized by six elastic constants, which are shown in Table 86.VI.

Figure 86.68 shows the variation of the Young’s modulus of a rod of KDP with orientation of the rod. The figure shows the unconstrained Young’s modulus E_u (i.e., when the only stress is in the direction of the rod, without any transverse stresses):

$$\frac{1}{E_u} = \frac{S_{13}}{4} + \frac{S_{44}}{8} + S_{33} \cos^4 \theta - \frac{2S_{13} + S_{44}}{8} \cos 4\theta + \left[S_{11} + \frac{(-2S_{11} + 2S_{12} + S_{66})}{4} \sin^2 2\phi \right] \sin^4 \theta, \quad (A1)$$

where θ is the angle between the direction of the rod and the cubic axis [001] and ϕ is the angle between the projection of the

rod axis on the (001) plane and the [100] direction. The Young’s modulus E_u varies from about 20 GPa to about 65 GPa. When averaged over all rod directions (i.e., integrated over the surface of a unit-radius sphere with differential element of area $dA = \sin \theta d\theta d\phi$), we find $\langle E_u \rangle = 35.5$ GPa.

Likewise, the constrained Young’s modulus E_c (where no strains transverse to the rod are allowed) is

$$E_c = \frac{C_{13}}{4} + \frac{C_{44}}{2} + C_{33} \cos^4 \theta - \frac{C_{13} + 2C_{44}}{4} \cos 4\theta + \left[C_{11} + \frac{(-C_{11} + C_{12} + 2C_{66})}{2} \sin^2 2\phi \right] \sin^4 \theta; \quad (A2)$$

E_c varies from about 40 GPa to 70 GPa, as shown in Fig. 86.68. When averaged over all directions, the result is $\langle E_c \rangle = 51.4$ GPa. The results in Fig. 86.68 clearly show that KDP is quite anisotropic.

To get a better idea of the elastic anisotropy, we can also determine the Reuss and Voigt averages as described by Hirth and Lothe,¹⁶ who summarize the earlier results by Hill.¹⁷ The Voigt averages for the shear modulus G_V and Lamé constant λ_V are given by

$$G_V = (3C_{ijj} - C_{iij})/30, \quad \lambda_V = (-C_{iij} + 2C_{ijj})/15, \quad (A3)$$

Table 86.VI: Elastic constants of KDP at 20°C.

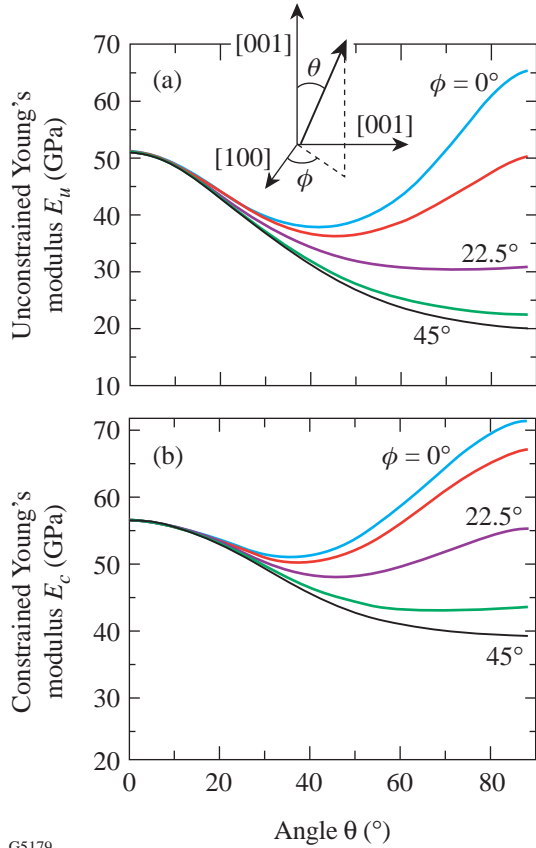
C_{11}	C_{33}	C_{12}	C_{13}	C_{44}	C_{66}
71.65	56.4	-6.27	14.94	12.48	6.21
Units of C_{ij} are GPa; data from Haussühl, ¹⁴ as cited in Milek and Neuberger. ¹ Stiffnesses C_{ij} relates stresses and engineering strains.					
S_{11}	S_{33}	S_{12}	S_{13}	S_{44}	S_{66}
1.51	1.95	0.18	-0.40	7.81	16.2
Units of S_{ij} are 1/(100 GPa); data from Hearmon, ¹⁵ as cited in Milek and Neuberger. ¹ Compliances S_{ij} relate engineering strains and stresses.					

where repeated indices are summed over the range $i, j = 1, 2, 3$. Here the constants C_{ijkl} relate the stress σ_{ij} and strain ϵ_{ij} tensors, $\sigma_{ij} = C_{ijkl} \epsilon_{kl}$. We thus find the average Young's modulus based on the Voigt scheme as $E_V = 44.3$ GPa. The corresponding Poisson ratio is $\nu_V = 0.23$.

The Reuss averages are given by

$$\frac{1}{E_R} = (2S_{ijj} + S_{iii})/15, \quad \frac{1}{G_R} = (6S_{ijj} - 2S_{iii})/15, \quad (A4)$$

where the constants S_{ijkl} relate the strain ϵ_{ij} and stress σ_{ij} tensors, $\epsilon_{ij} = S_{ijkl} \sigma_{kl}$. We find the Reuss average of the Young's modulus $E_R = 33.0$ GPa. The corresponding Poisson ratio is $\nu_R = 0.30$.



G5179

Figure 86.68
Variation of Young's modulus of KDP with crystallographic orientation. The Young's modulus is the ratio of stress to strain for a rod making angles θ, ϕ with the crystallographic axes and stretched in the direction of the rod. Unconstrained E_u corresponds to no transverse stresses acting on the rod. Constrained E_c is valid when the rod is not allowed to strain in the transverse directions.

REFERENCES

1. S. Anbukumar, S. Vasudevan, and P. Ramasamy, *Indian J. Phys. A* **61A**, 397 (1987).
2. G. R. Anstis *et al.*, *J. Am. Ceram. Soc.* **64**, 533 (1981).
3. R. F. Cook and G. M. Pharr, *J. Am. Ceram. Soc.* **73**, 787 (1990).
4. A. G. Evans, in *Fracture Mechanics Applied to Brittle Materials*, edited by S. W. Freiman (American Society for Testing and Materials, Philadelphia, 1979), Vol. ASTM STP 678, Part 2, pp. 112–135.
5. C. H. Guin *et al.*, *Krist. Tech.* **15**, 479 (1980).
6. R. F. S. Hearmon, *Br. J. Appl. Phys.* **3**, 120 (1952).
7. S. Haussühl, *Z. Kristallogr.* **120**, 401 (1964).
8. R. Hill, *Proc. Phys. Soc.* **65A**, 349 (1952).
9. J. P. Hirth and J. Lothe, *Theory of Dislocations*, 2nd ed. (Wiley, New York, 1982), Chap. 13, Sec. 13.2, pp. 424–428.
10. K. K. Rao and D. B. Sirdeshmukh, *Indian J. Pure Appl. Phys.* **16**, 860 (1978).
11. J. C. Lambropoulos, T. Fang, P. D. Funkenbusch, S. D. Jacobs, M. J. Cumbo, and D. Golini, *Appl. Opt.* **35**, 4448 (1996).
12. J. Lankford, *J. Mater. Sci. Lett.* **1**, 493 (1982).
13. J. E. Marion, *J. Appl. Phys.* **62**, 1595 (1987).
14. J. T. Milek and M. Neuberger, *Linear Electrooptic Modular Materials*, Handbook of Electronic Materials, Vol. 8 (IFI/Plenum, New York, 1972), pp. 177–222.
15. C. B. Ponton and R. D. Rawlings, *Mater. Sci. Technol.* **5**, 865 (1989).
16. *ibid.*, p. 961.
17. M. P. Shaskol'skaya, H.-K. Ch'ang, and M. D. Katrich, *Izv. Akad. Nauk SSSR Neorg. Mater.* **14**, 716 (1978).